www.ietdl.org

Published in IET Nanobiotechnology
Received on 14th March 2011
Revised on 8th June 2011
doi: 10.1049/iet-nbt.2011.0018

Special Issue – selected papers from the NEMS conference 2011

ISSN 1751-8741

Digital microfluidic operations on micro-electrode dot array architecture

G. Wang[1] *D. Teng*[2] *S.-K. Fan*[2]

[1]*Department of Electrical and Computer Engineering, University of Saskatchewan, 57 Campus Drive, Saskatoon, SK, Canada S7N 5A9*
[2]*Department of Materials Science and Engineering, National Chiao Tung University, 207 Engineering 1, 1001 University Road, Hsinchu, Taiwan*
E-mail: gary.wang@usask.ca; gary.cj.wang@gmail.com

Abstract: As digital microfluidics-based biochips find more applications, their complexity is expected to increase significantly owing to the trend of multiple and concurrent assays on the chip. There is a pressing need to deliver a top-down design methodology that the biochip designer can leverage the same level of computer-aided design support as the semi-conductor industry now does. Moreover, as microelectronics fabrication technology is scaling up and integrated device performance is improving, it is expected that these microfluidic biochips will be integrated with microelectronic components in next-generation system-on-chip designs. This study presents the analysis and experiments of digital microfluidic operations on a novel electrowetting-on-dielectric-based 'micro-electrode dot array architecture' that fosters a development path for hierarchical top-down design approach for digital microfluidics. The proposed architecture allows dynamic configurations and activations of identical basic microfluidic unit called 'micro-electrode cells' to design microfluidic components, layouts, routing, microfluidic operations and applications of the biochip hierarchically. Fundamental microfluidic operations have been successfully performed by the architecture. In addition, this novel architecture demonstrates a number of advantages and flexibilities over the conventional digital microfluidics in performing advanced microfluidic operations.

1 Introduction

Historically, microfluidic devices have been designed from bottom up, whereby various fluidic components are combined together to achieve a device that performs a particular application. Therefore microfluidic systems built to date are realised in custom technologies that may not be widely available. As more bioassays are expected to be executed concurrently on a lab-on-a-chip (LOC), more sophisticated control for resource management, system integration and design complexity are expected to increase dramatically. Current full-custom design and fabrication techniques do not scale well for the challenge. There is a pressing need to deliver a top-down design methodology that LOC designers can leverage the same level of computer-aided design support as the semi-conductor industry now does. One viable approach will be a validated and easy-to-operate microfluidic platform that can be easily programmed to build application-specific microfluidic systems, similar to the development of application-specific integrated circuits (ASICs). Indeed, a hierarchical integrated microfluidic design approach has been described to facilitate scalable design for biomedical applications [1, 2]. However, more important than providing a complete set of validated microfluidic elements within a platform is the fact that all elements have to be amenable to a well-established fabrication technology. Lacking of standard fabrication technologies and microfluidic component libraries makes the hierarchical ASIC-like design approach difficult to implement for microfluidic devices.

Scalability, configurability and portability of fundamental building elements hold the key to the success of hierarchical design of digital microfluidics. To achieve scalability and configurability of digital microfluidics, we propose a micro-electrode dot array (MEDA) architecture. Unlike other digital microfluidics system where fixed-sized electrodes are arranged in an array or a certain pattern to perform a set of predefined bioassay, this proposed architecture is based on the concept of sea-of-micro-electrodes array where an array of identical basic microfluidic unit components called 'micro-electrode cells'. Each micro-electrode cell consists of a micro-electrode and a control/activation circuit. Similar to metal–oxide–semi-conductor field-effect transistors to implement logic gates and other digital circuits found in computers, telecommunications equipment and signal processing equipment, this proposed architecture, hereafter referred to as 'MEDA architecture', allows micro-electrode cells to implement microfluidic components and microfluidic operations for LOC's. The architecture can be realised using commonly available fabrication technologies specifically the complementary metal-oxide-semi-conductor (CMOS) technology. A micro-electrode cell can be implemented as a CMOS standard cell which is a group of CMOS transistors, interconnect structures and a physical micro-electrode. Standard cell-based methodology makes it possible for one designer to focus on the high-level

© The Institution of Engineering and Technology 2011

(function) aspect of LOC design, whereas another designer focuses on the implementation (physical) aspect. One good example is that along with semi-conductor manufacturing advances, standard cell methodology has helped designers scale ASICs from comparatively simple single-function ICs (of several thousand gates), to complex multi-million gate system-on-a-chip devices.

Many potential applications can be implemented by MEDA architecture. For example, based on MEDA architecture and CMOS technology, a field-programmable LOC (FPLOC) is feasible and can significantly leverage existing computer-aided design tools and support for ASICs and field-programmable gate array. Graphical programming language such as National Instrument's LabVIEW can be leveraged to have an FPLOC add-in module available to target and program FPLOC hardware. The graphical programming language approach drastically simplifies the FPLOC programming process. In addition, as MEDA architecture fostering a development path for a large-scale integration of microelectronic components into microfluidic biochips, an integrated droplet monitoring circuitry which can detect the locations of all existing droplets on the LOC will be feasible. One step further, an integrated ultra-sensitive CMOS impedimetric sensor and other biosensors will be possible. This paper presents the initial implementations and experimental results of our effort towards MEDA architecture.

2 MEDA architecture

2.1 Fundamental electrowetting-on-dielectric operations

A number of methods for manipulating microfluidic droplets have been proposed in the literature. These techniques can be classified as chemical, thermal, acoustical, magnetic and electrical methods. Among all methods, our focus is on electrowetting-on-dielectric (EWOD) which is not only one of the most common electrical methods but also the most compatible to the standard CMOS technology. EWOD takes advantage of electrohydrodynamic forces, and they can provide high droplet speeds with relatively simple geometries. A hydrodynamic scaling model of droplet actuation was constructed in a systematic manner and was concluded that reliable operation of an EWOD actuator is possible as long as the device is operated within the limits of the Lippmann–Young equation [3]. This scaling design framework provides the base of MEDA architecture. The Lippmann–Young equation (1) is derived from the Lippmann's equation [4] and Young's equation [5]. The change of contact angle by the electric potential, V, can be described as

$$\cos\theta(V) - \cos\theta_0 = \frac{\varepsilon_0\varepsilon}{2\gamma_{LG}t}V^2 \quad (1)$$

where $\theta(V)$ is the contact angle when a potential is applied, θ_0 denotes the equilibrium contact angle at $V = 0$ V, ε_0 (8.85×10^{-12} F/m) is the permittivity of vacuum, ε is the dielectric constant of the dielectric layer, γ_{LG} the liquid–gas interfacial tension and t is the thickness of the dielectric layer. For droplet motion, a certain contact angle difference is required by applying adequate drive voltage. Note in the Lippman–Young equation, the contact angle change is not related to the polarity of the applied potential, V.

MEDA architecture can be designed by using scaled-down electrodes based on EWOD. A typical configuration of EWOD uses two parallel plates (i.e. bi-planer structure) [6, 7]. An MEDA architecture chip with bi-planer structure is shown in Fig. 1: a top plate with a fixed blanket referencing electrode and a bottom plate with patterned addressable driving micro-electrodes. Micro-electrodes are covered with a dielectric layer (e.g. SiO_2), which is, in turn, coated with a hydrophobic layer (e.g. Teflon and Cytop). The top reference electrode is essential for stable actuation since it provides the ground for the potential drops across insulating layers. A liquid droplet is sandwiched between the two plates, forming the initial droplet shape. Once electrical potential is applied between the top reference electrode and the bottom driving electrode, the EWOD effect causes an accumulation of charge in the droplet/insulator interface, resulting in an interfacial tension gradient across the gap between the adjacent electrodes, which consequently causes the transportation of the droplet.

2.2 Hierarchical structure

Each micro-electrode cell consists of a micro-electrode and a control/activation circuit. A block diagram of an LOC based on MEDA architecture and CMOS fabrication technology is illustrated in Fig. 2. The two main blocks are the system control block and the micro-electrode cell. Normally, a system has only one system control block but a plurality of micro-electrode cells depending on the applications and the limitation of the fabrication technologies. Micro-electrode cells are daisy-chained together to simply the wiring and to maximise the scalability. One micro-electrode cell is composed of a high-voltage driving micro-electrode, 1-bit cell data and control circuits. The high-voltage driving micro-electrode is the physical micro-electrode that can be activated by a high-voltage driver to cause the EWOD effect to move the droplet as illustrated in Fig. 1. The 1-bit cell data holds the logic value of the activation of the micro-electrode that typically a 'one' means activation and a 'zero' means deactivation of the micro-electrode. Every activation cycle starts with shift-loading the 1-bit cell data into all micro-electrode cells and then voltage in (VIN) signal activates the high-voltage driver to apply driving voltages to physical micro-electrodes. The control circuit manages the control logics, the high-voltage driver and forms the daisy-chain structure of the micro-electrode cells.

Depending on fabrication technologies and application needs, the system controller can be entirely or partially integrated into the LOC. The controller has a CPU with enough memory space, interface circuitries and software programmability. The chip layout map stores configuration data of the layout of the chip and the designs of

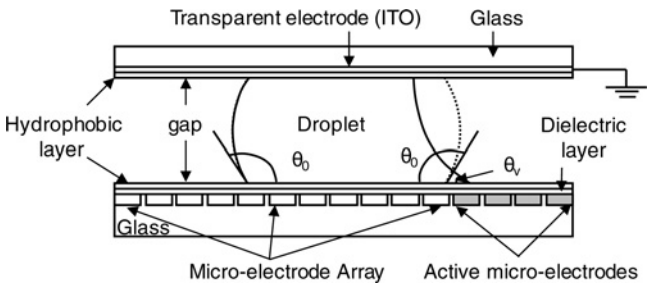

Fig. 1 *Illustration of the MEDA architecture by using scaled-down electrodes based on EWOD bi-planer structure (not to scale)*

© The Institution of Engineering and Technology 2011

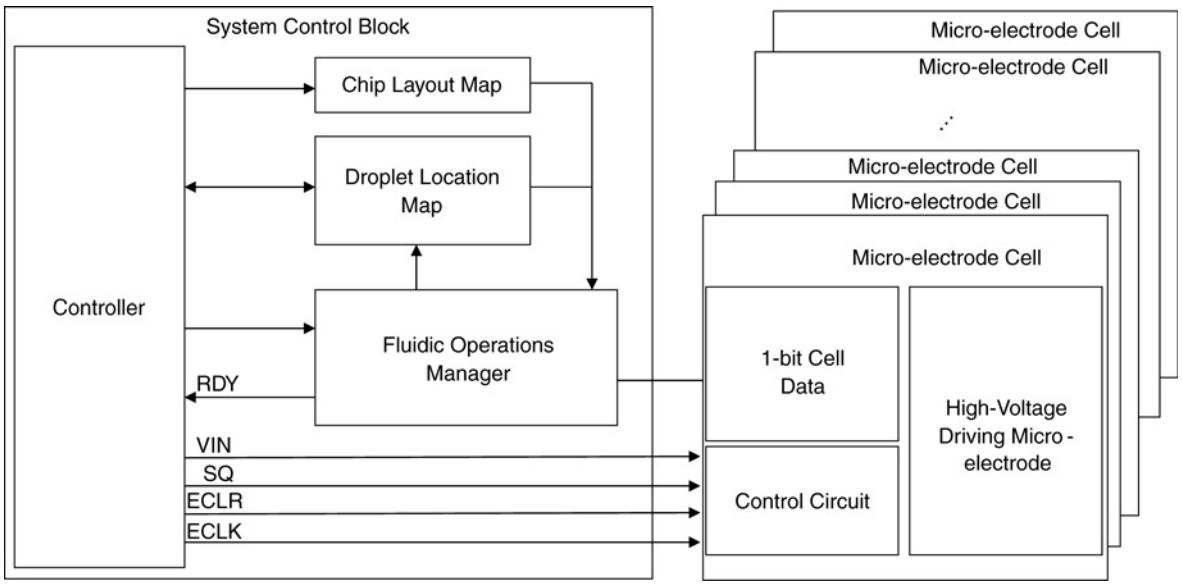

Fig. 2 *Block diagram of an LOC based on MEDA architecture and CMOS fabrication technology*

microfluidic components. The droplet location map reflects the real-time locations and other parameters of the droplets on the LOC. The fluidic operations manager translates the layout map, the droplet location map and the LOC applications from the controller into a map of 1-bit cell data. Physical actuations are performed by shift-loading the 1-bit cell data into micro-electrode cells followed by activating the high-voltage driver.

Hierarchically, micro-electrode cells form the foundation of building the entire LOC as indicated in Fig. 3*a*. A top-down design methodology of LOCs starts from the biomedical microfluidic functions layer. At this layer, application-level functions and the purposes of the LOCs are defined. For example, one LOC could perform one function such as glucose reading or multiple analyses such as a 12-in-1 drug-of-abuse check.

Microfluidic operations is one level down layer that controls and manages the microfluidic operations such as transportation, mixing and detection. After the biomedical microfluidic functions have been defined then architectural-level synthesis is used to convert the microfluidic functions to LOC resources and to map the microfluidic functions to the time steps. Ideally, both biomedical microfluidic functions and microfluidic operations are a methodology of design abstraction, whereby a low-level micro-electrode configuration and layout is encapsulated into an abstract microfluidic representation [such as 'diagonal cutting' or 'split-and-recombine (SAR) lamination mixing']. Along with microfluidics advances, this top-down methodology will be responsible for allowing designers to scale digital microfluidic system from comparatively simple single-function LOCs, to complex multi-function LOCs.

At the microfluidic components layer, geometry-level synthesis creates a physical representation of the final layout of the LOC at the geometrical level. The final layout includes the locations of all microfluidic components, the shapes and sizes of the microfluidic components, the configuration of the micro-electrode array and other geometric details as indicated by Figs. 3*b* and *c*.

Finally, the micro-electrode arrays layer is the foundation of this hierarchical structure. Micro-electrode array can be physically implemented in many different ways but the physical electrode is just a portion of the architecture. Other architecture considerations to provide accurate

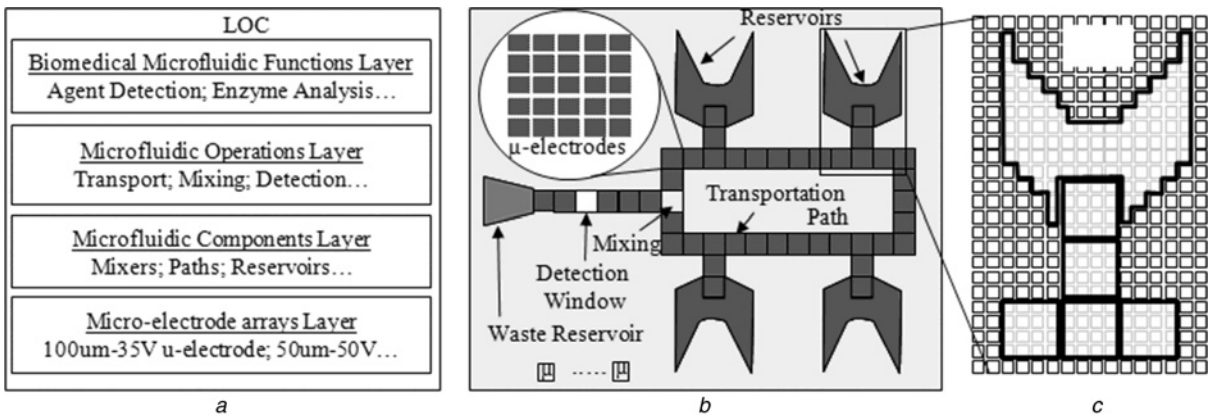

Fig. 3 *MEDA architecture*

a Hierarchical structure of MEDA architecture
b Example of the final layout
c Illustration of an enlarged portion of the micro-electrode array

© The Institution of Engineering and Technology 2011

doi: 10.1049/iet-nbt.2011.0018

three-dimensional geometrical modelling and physical-level simulation should also be included, such as daisy-chained structure and self-contained structure. A daisy-chained structure can significantly simplify the wiring of micro-electrode cells that a consistent interconnection of each micro-electrode cell can maximise the scalability of MEDA architecture. Another important design of MEDA architecture is the self-contained micro-electrode structure that all control circuit, flip-flops, and high-voltage driver are contained in the area directly beneath the physical micro-electrode. This self-contained microelectrode structure is essential to provide accurate 3D geometrical modelling and physical-level simulation that is the key to complete top-down design automation. Also, this self-contained structure has the great scalability in the fabrication of microelectrode arrays.

2.3 Effective length of the contact line

The shape of micro-electrode can be physically implemented in different ways. However, exact modelling and simulations of droplet motion in EWOD are complicated [8]. By careful examination of the MEDA architecture, we believe the gaps among discrete micro-electrodes impose an uncertainty on the architecture. When a droplet is in contact with a solid surface, the interaction among molecules of the droplet, the ambient fluid and the solid can lead to a net force of attraction (wetting) or repulsion (non-wetting). The wetting force denoted f_w, is a line force density defined by the following expression [9]

$$f_w = \gamma_{LG} \cos \theta(V) \tag{2}$$

where γ_{LG} is the liquid–gas interfacial tension and $\theta(V)$ is the contact angle when a potential is applied. f_w acts on the tri-phase contact line, and is in plane with the solid surface, perpendicular to the tri-phase contact line and points away from the droplet.

From (2), it can be shown as in Fig. 4*a* that the capillary force F_x acting on the droplet in the direction of unit vector $\boldsymbol{i}$ is expressed as [10–12]

$$F_x = \gamma_{LG} \cos \theta(V) \int_L \mathrm{d}l n \cdot \boldsymbol{i} = \gamma_{LG} \cos \theta(V) e \tag{3}$$

where dl is a unit element of the droplet contour line and n is the unit normal to the contour line and e is the effective length of the contact line as indicated in Fig. 4*a*.

From (3), it is apparent that the magnitude of the capillary force is determined only by the effective length of the contact line, for example, it is independent of the shape of the contact line. So the two different shapes of droplets shown in Fig. 4*b* have the same effective length and have the same capillary force on the droplets.

However, the shapes of the contact lines do have an effect on the MEDA architecture because of the gaps between micro-electrodes. Fig. 5 illustrates three different shapes and layouts of micro-electrode arrays, one is hexagon micro-electrode and the other two are square electrodes with different layouts. As indicated in the figures, the effective lengths (e) of the contact lines have the impact from the gaps among micro-electrodes. According to this simplified model, the total capillary force exerted on droplets in MEDA architecture was expected to be reduced as a result of the gaps among discrete micro-electrodes. Table 1 shows

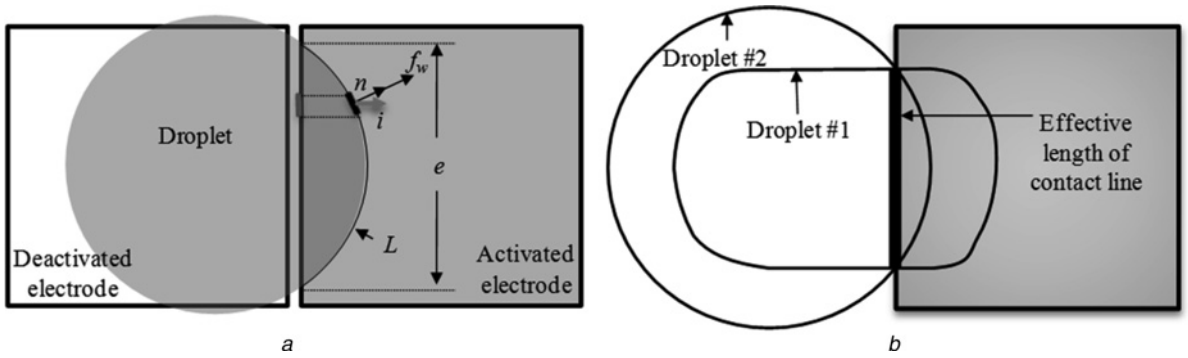

Fig. 4 *Capillary force acting on the droplet*

a Contact line and the capillary force acting on the droplet in direction of unit vector $\boldsymbol{i}$
b Two different shapes of droplets have the same effective length and have the same capillary force on the droplets

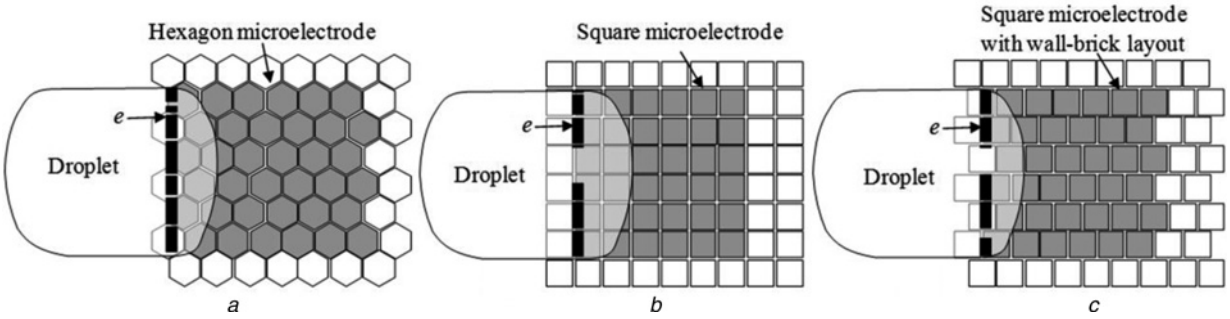

Fig. 5 *Different effective contact lines by three different shapes and layouts of micro-electrode arrays*

a Effective contact line of hexagon micro-electrode
b Effective contact line of square micro-electrode
c Effective contact line of square micro-electrode with wall-brick layout

© The Institution of Engineering and Technology 2011

Table 1 Comparisons of the travelling time of different micro-electrode types are related to a solid electrode

Time to move to the next electrode (distance = 1100 μm)										
		1 KHz, square	ms	Micro-electrode type			%	Micro-electrode type, %		
Gap, μm	Aspect ratio	Vp-p	Solid	Square	Hexagon	Wall_S	Solid	Square	Hexagon	Wall_S
100	0.092	100	100.00	183.33	161.11	175.00	100	55	62	57.14
		96	147.22	275.00	209.72	230.56	100	54	70	63.86
		92	173.61	377.78	284.72	313.89	100	46	61	55.31
80	0.073	100	129.17	202.78	187.04	202.78	100	64	69	63.70
		96	161.11	266.67	230.56	236.11	100	60	70	68.24
		92	195.83	316.67	304.63	333.33	100	62	64	58.75
40	0.037	100	158.33	416.67	202.78	205.56	100	38	78	77.03
		96	213.89	580.56	286.11	316.67	100	37	75	67.54
		92	306.94	305.56	427.78	452.78	100	38	72	67.79
20	0.018	100	209.72	577.78	350.99	441.67	100	36	60	47.48
		96	275.69	769.44	469.86	597.22	100	36	59	46.16
		92	393.75	1172.22	726.74	908.33	100	34	54	43.35

Percentage numbers are the speed ratios of the micro-electrode and the solid electrode

the comparison of the times (ms) to travel a distance of 1.1 mm by different shapes of micro-electrodes to a solid electrode. The reduced force should be compensated by maximising the length of the effective contact line, such as the interdigitated electrodes proposed by Jang *et al.* [12], at all times. Therefore in optimising the performance of EWOD, it is believed that an electrode being configured with a cluster of micro-electrodes in such a way that the flexibility of micro-electrodes does not adversely affect EWOD operations.

2.4 Aspect ratio and cover structure considerations

As the diameters of the electrodes can be dynamically configured for MEDA architecture and the sizes of the configured-electrodes can be varied greatly, guidelines of aspect ratios of MEDA architecture including different cover structures will be needed. Typically, a bi-planar structure is used by LOC designers, but the coplanar design removes the electrical connection to the cover and can accommodate more sensing mechanisms from above and thus allows increased flexibility for system development. MEDA architecture can accommodate both coplanar and bi-planar structure. By configuring some of the micro-electrodes as the ground electrodes, a coplanar structure can be easily implemented by MEDA architecture. As droplet minimum splitting voltages exceed the minimum voltages for dispensing and transport in bi-planar structures. The relation between splitting voltages and aspect ratio, d/L, drives the aspect ratio design guidelines for MEDA architecture. The general MEDA architecture design guidelines are: (i) keep $d/L < 1$ for an oil medium and (ii) keep $d/L < 0.4$ for an air filler medium [3]. The main purpose for the guidelines is to ensure that the minimum splitting voltage for an actuator less than the saturation voltage (V_{sat}). However, more uniform splitting places tighter limits on the actuator aspect ratio [3]. By following the aspect ratio design guidelines, our experiments have been performed smoothly in all microfluidic operations.

Our experiments generally agree with the first scaling rule for an EWOD actuator from the scaling model by Song *et al.* [3] that says increasing d/L with all other variables fixed increases droplet velocity up to a maximum, although the dependence on d/L is weak. Nonetheless, the percentage numbers in Table 1, which are speed ratios between the micro-electrodes and the solid electrode, show the best percentage numbers of square micro-electrode at $d/L = 0.073$ and the best percentage numbers of hexagon and wall_square at $d/L = 0.037$. The comparison to the solid electrode is to remove other variables not related to the geometric shapes of micro-electrodes. We believe that the speed dependence is also on the combination of the geometric shapes of the droplets and micro-electrodes. The aspect ratio varies the travelling shapes of the droplets and consequently changes the effective lengths of the contact lines. A lower aspect ratio typically makes the droplet squarer and a squarer droplet has bigger impact on the square micro-electrode as illustrated in Fig. 5*b*. As expected, the test results show significant performance degradation of the square micro-electrode when $d/L \leq 0.037$.

3 Proof-of-concept experiments

To prove the concept of the MEDA architecture as well as to demonstrate the flexibility and to investigate any potential problems of the MEDA architecture, a number of prototypes are fabricated on indium tin oxide (ITO) glasses to conduct extensive experiments of EWOD operations. The test structures were fabricated on ITO glasses based on the square micro-electrode as illustrated in Fig. 5*b* to simulate the worst-case scenario. Each micro-electrode is 100 μm × 100 μm with 10 μm gaps between micro-electrodes. Both 2 × 12 and 4 × 12 individually controllable micro-electrode arrays are fabricated for simple configuration tests. The design of the 4 × 12 micro-electrode array is shown in Fig. 6*a*. For more complicated group activations, different groups of micro-electrodes are hardwired together to simulate the group-activation for the experiments. Fig. 6*b* is the ITO glass design for performing the diagonal transport and cutting. The connection trace is 10 μm wide. A layer of 1 μm SU8-2002 was spin coated (1000 RPM for 5 s and then 4500 RPM for 60 s) on top of ITO glass for the dielectric layer and followed by 90°C soft bake, 2.5 s exposure (~36 mW/cm^2) and 150°C 30 min bake. After the dielectric layer, 1% Teflon AF1600 was spin coated (3000 RPM) on the glass and then baked for 30 min at 150°C.

© The Institution of Engineering and Technology 2011

doi: 10.1049/iet-nbt.2011.0018

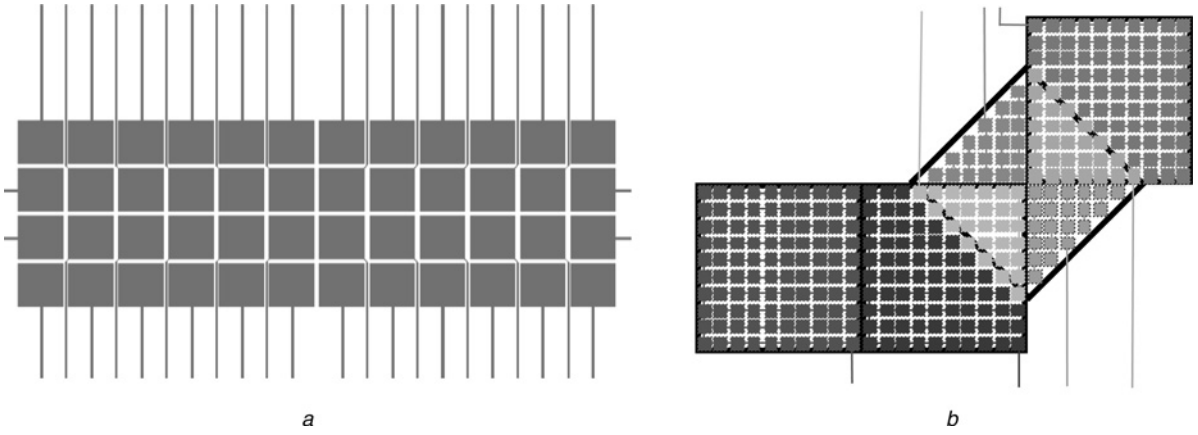

Fig. 6 *Fabrication of ITO glasses*

a Is the picture of the 4 × 12 individually controllable micro-electrode array
b Is the ITO glass design for performing the diagonal transport and cutting

Fundamental EWOD microfluidic operations have been verified successfully. In addition, many advanced microfluidic operations that only can be achieved by MEDA architecture have been performed and evaluated through the experiments.

3.1 Droplet dispensing

Droplet dispensing refers to the process of generating droplets from on-chip reservoirs. Fig. 7 shows the creation of droplets of de-ionised (DI) water in two different experiment settings. Fig. 7*a* shows the pinching droplet from the reservoir for a typical droplet dispensing. Here, each of the configured-electrodes is composed of 10 × 10 micro-electrodes and the reservoir is composed of 24 × 26 micro-electrodes. There are no vertical walls for the droplet dispensing. Also, because of the dynamic activation capability of the micro-electrodes of the reservoir, dispensing operation is able to work regardless the volume of liquid in the reservoir.

Fig. 7*b* illustrates a special droplet dispensing procedure called 'droplet-aliquots'. MEDA architecture can create smaller droplets (the aliquot droplet) from reservoir by first activating calculated micro-electrodes (3 × 3 micro-electrodes in this case) and then collecting the calculated numbers of aliquot droplets together by activating a bigger electrode (10 × 10 micro-electrodes in this case) to form a controlled-volume droplet. Conventionally, droplet sizes are approximated to the sizes of the electrodes but a easy and more precise way to control the volumes of the droplets does not exist. Droplet-aliquots can be used for a more precise control of the volumes of the droplets. Also, in a reverse way, this technique can be used to measure the volume of a droplet, in a way to count how many smaller aliquot droplets can be created from the bigger one.

3.2 Droplet transport

Droplet transport is a well-established microfluidic operation. Droplet transport in bi-planar, in coplanar (where electrodes and ground are on the same plate) with cover and in coplanar without cover have been successfully evaluated with MEDA architecture [13].

Fig. 8*a* indicates a diagonal transport that cannot be performed by the conventional EWOD operation because there is no physical contact between the droplet and the targeted electrode. By using the dynamic configurability of MEDA architecture, an interim step as depicted in the dotted area in Fig. 8*a* can be implemented easily. Fig. 8*b* shows the overlaid picture of a smooth diagonal droplet move with the help of the interim step. Although simple in principle, the capability to move droplets in any direction has a profound advantage on the routing of the droplets.

Droplets decrease in sizes because of cutting or evaporation, and sometimes cannot be actuated reliably by electrodes. Interim bridging technique can easily resolve the issue. The interim bridging technique is used to overcome the physical gap that prevents a normal droplet move from electrode 1 to electrode 2 as shown in Fig. 8*c*. The interim bridging can be implemented in many different shapes. Four micro-electrodes in green are added to electrode 2 to form the interim bridging. This interim bridging technique also demonstrates the capability of MEDA architecture to

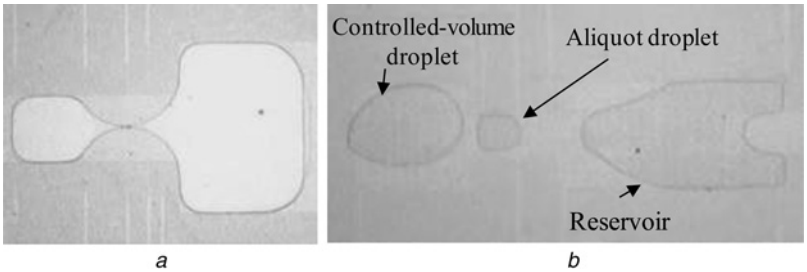

Fig. 7 *Creation of droplets of DI water in two different experiment settings*

a Typical droplet dispensing by MEDA architecture (bi-planar with 80 μm gap between two plates, DI water in air, 40 Vp-p, 1 kHz square wave)
b Droplet aliquots (bi-planar with 20 μm gap, DI water in 10 cSt silicone oil, 50 Vp-p 1 kHz square)

© The Institution of Engineering and Technology 2011

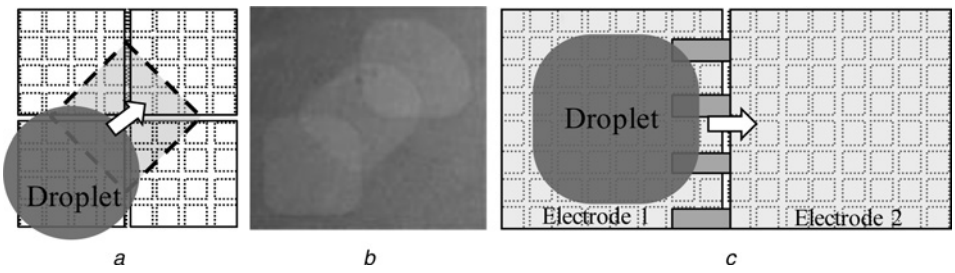

Fig. 8 *Dynamic configurability of MEDA architecture*

a Diagonal droplet move by an interim step as depicted in the dotted area
b Overlaid picture of a diagonal droplet move
c Interim bridging technique is used to overcome the physical gap that prevents a normal droplet move from electrode 1 to electrode 2

configure micro-electrodes into interdigitated electrodes to have better effective length of the contact line and as a result to improve the performance of the transport as suggested by Jang *et al.* [12].

Electrode column actuation is another effective way to flush out the stuck droplets. As shown in Fig. 9*a*, the actuating electrodes are arranged into columns to perform the electrode column actuation. Here, each electrode column is composed of 1 × 10 micro-electrodes and five electrode columns are grouped together to perform the column actuation. For these 5 × 10 micro-electrodes to move a droplet, the column in front of the leading column is activated whereas the trailing column is deactivated. Our experiments showed that under marginal driving voltages, the electrode column actuation provides very smooth and effective driving capability because the effective contact line is consistent and maximised as illustrated in Fig. 9*a*. A droplet of about 8 × 8 micro-electrode size is moved by the electrode column actuation as shown in Fig. 9*b*. Fig. 9*c* shows the electrode column actuation of a smaller droplet of about 4 × 4 micro-electrdoe size.

3.3 Cutting

For cutting a droplet, typically three electrodes are used. During cutting, the outer two electrodes are activated and with the inner electrode deactivated. Fig. 10*a* shows a typical cutting performed by three 1.1 mm × 1.1 mm configured-electrodes. Each configured-electrode has 10 × 10 micro-electrodes. A diagonal cutting is an advanced cutting that can be performed easily with the MEDA architecture as illustrated in Figs. 10*b* and *c*. In general, the diagonal cutting is more effective than the conventional cutting because the two pulling electrodes provide more effective contact lines with the droplet as indicated in Fig. 10*b*. Also, the diagonal cutting is less constrained by the droplet size. A conventional three-electrode cutting requires a droplet to be big enough to touch the two outer electrodes. A diagonal cutting can virtually cut any sizes of droplets.

3.4 Mixing

A droplet acts as a virtual mixing chamber. Droplet mixing occurs by transporting two droplets across an electrode array into an electrode. Fowler *et al.* [14] proposed a simple movement pattern in bi-planar EWOD devices to mix drops in air. Our research focus is on the manipulations of the micro-electrode array to create SAR lamination mixing to achieve fast mixing by using as small area as possible. This SAR lamination mixer is especially useful at a low-Reynolds-number situation.

Three basic steps are required for SAR lamination mixing: fluid element splitting, recombination and rearrangement. The concept of stretching and folding of stretching and cutting can be captured by means of the so-called baker's transformation [15]. After one SAR cycle, the two lamellae can be split into four lamellae. Then, the interfacial contact area is increased by double and the diffusion length is reduced to a half. The lamellae dimension depends on the number of SAR cycles (n). The diffusion length after n SAR steps leads to an exponential decrease of $1/2^n$; and exhibits an exponential increase of the interfacial contact area. Figs. 11*a*–*f* illustrate a small footprint (2 × 2 configured-electrodes) SAR lamination mixer based on MEDA architecture. Fig. 11*a* illustrates the initial positions of the black droplet and the white droplet. To start the SAR lamination mixing, step one is to merge the two droplets diagonally as illustrated in

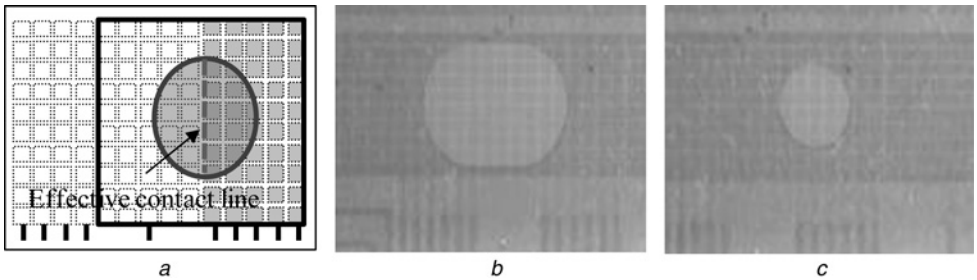

Fig. 9 *Electrode column actuation*

a Each electrode column is composed of 1 × 10 micro-electrodes and five electrode columns are grouped together to perform the column actuation. The consistent and maximised effective contact line provides very smooth and effective driving capability
b Droplet of about 8 × 8 micro-electrode size is moved by the electrode column actuation
c Electrode column actuation of a smaller droplet of about 4 × 4 micro-electrdoe size

© The Institution of Engineering and Technology 2011

doi: 10.1049/iet-nbt.2011.0018

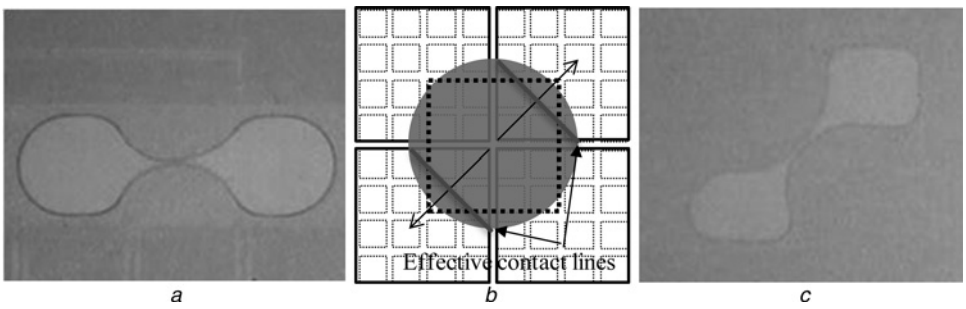

Fig. 10 *Cutting*

a Cutting (bi-planar with 100 μm gap, DI water in air, 62 V 1 kHz square)
b Effective contact lines during diagonal cutting
c Diagonal cutting (DI water in air, bi-planar with 40 μm gap, 44 V 1 kHz square)

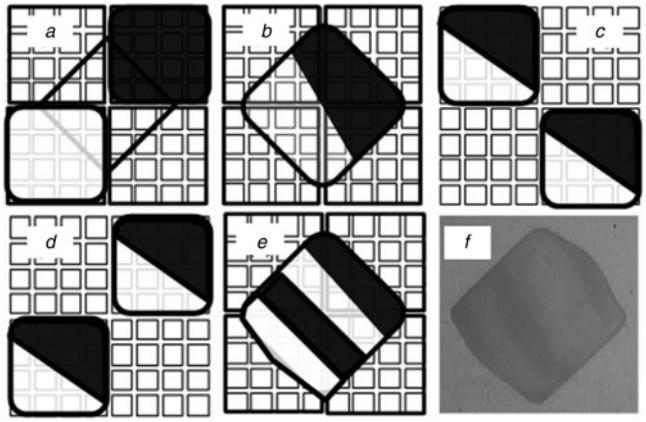

Fig. 11 *SAR lamination mixing based on the MEDA architecture*

a Initial positions of the droplets
b–e Baker's transformation [15]
f Picture from the experiment after one SAR lamination mixing cycle

Fig. 11*b*. The second step is to do the diagonal cutting which is 90° from the diagonal mixing as illustrated in Fig. 11*c*. Then, the third step of the SAR lamination mixing is to move the two droplets back onto the starting configured-electrodes to repeat the diagonal mixing and cutting as illustrated in Fig. 11*d*. The procedure of steps 1–3 can be repeated to create the necessary numbers of lamellae to speed up the mixing. Fig. 11*e* illustrates the four lamellae of the droplet repeating after one SAR lamination mixing cycle and Fig. 11*f* is the picture from our experiment. Typically, after three cycles of the SAR lamination mixing the droplet is well mixed.

3.5 EWOD channel-based actuation

EWOD channel-based actuation is another very simple in control but very effective way of doing microfluidic operations implemented by MEDA architecture. As shown in Fig. 12, a channel between the targeted electrode and the reservoir can be formed with a line of micro-electrodes. While reservoir is deactivated, the activation of both the channel and the targeted electrode cause a liquid flow from the reservoir into the channel and the targeted electrode as shown in Fig. 12*a*. Once the targeted electrode is filled up, the liquid flow stops as shown in Fig. 12*b*. Then the bridge is deactivated first to cut the linkage and subsequently the liquid in channel is pulled back to the activated reservoir. The deactivation of the channel typically starts from the micro-electrode adjacent to the targeted electrode to prevent extra liquid pulled into the targeted electrode. In the experiment, the bridge is a single line of 100 μm × 100 μm micro-electrode with 10 μm gaps between micro-electrodes. The targeted electrode is composed of 10 × 10 micro-electrodes and the reservoir is composed of 10 × 20 micro-electrodes.

Although this experiment looks simple but it actually covers all four fundamental microfluidic operations: dispensing, transport, mixing and cutting. As described above, a 10 × 10 micro-electrode droplet has been dispensed from a 10 × 20 micro-electrode reservoir. On the other hand, it could be interpreted as a 10 × 20 micro-electrode droplet being cut into two 10 × 10 micro-electrode droplets by the channel actuation. The channel is formed to transport liquid from the reservoir to the targeted electrode. For a longer channel, the liquid might have to move as a controlled-length snake but not fulfiling the entire channel. The digital nature of MEDA architecture provides many advantages in the dynamic configuration of the channel and the control of the liquid volume. The channel actuation is also very useful in solving some droplet routing issues because small channels can be configured to share the bottleneck area. For example, a configured-electrode is composed of 10 × 10 micro-

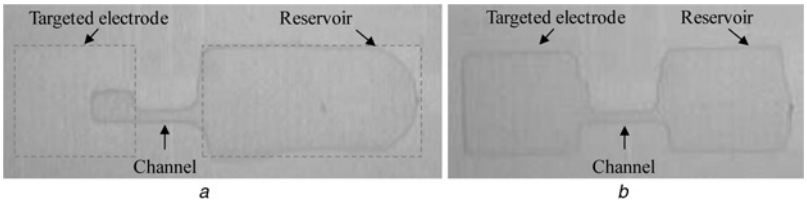

Fig. 12 *EWOD channel-based dispensing and cutting*

a Liquid starts to flow from reservoir into the channel and the targeted electrode (bi-planar with 20 μm gap, DI water in 10 cSt silicone oil, 50 Vp-p 1 kHz square)
b Liquid flow stops when the targeted electrode is filled up

© The Institution of Engineering and Technology 2011

electrodes and two droplets need to move through the same configured-electrode. To avoid contamination, two channels can be configured and the channel actuation is used to move through the congested area and then two droplets being regrouped at uncongested space. Different channels can be formed to move liquid from different sources into the same targeted electrode (mixing chamber) to do mixing. Once the channels are deactivated, if needed, a SAR lamination mixer can be implemented to speed up the mixing.

4 Conclusion

This paper characterised and identified an MEDA architecture that fosters hierarchical integrated microfluidic design approach. The capability of dynamic configuration of variable shapes and sizes of the electrodes and dynamic manipulation of droplets opens the possibility of a real field-programmable and reusable digital microfluidic system. Analysis and experiments have been done to address the key uncertainties, the gaps among the micro-electrodes, of the architecture. Fundamental EWOD microfluidic operations have been verified successfully with ITO glass-based prototypes to simulate the worst-case scenario. It was believed that an electrode be configured with a cluster of micro-electrodes in such a way that the flexibility of micro-electrodes does not adversely affect EWOD operations. In addition, many advanced microfluidic operations that only can be achieved by the MEDA architecture have been demonstrated. Future research effort will be focused on the implementation of a LOC based on the MEDA architecture that is amenable to well-established CMOS fabrication technologies.

5 Acknowledgments

The authors are grateful for the support of Department of Materials Science and Engineering, National Chiao Tung University (NCTU), Taiwan. All experiments and fabrications for proof of the concept presented in this paper were performed at the FAN-TASY Lab at NCTU.

6 References

1 Fair, R.B.: 'Digital microfluidics: is a true lab-on-a-chip possible?', *Microfluid Nanofluid*, 2007, **3**, (3), pp. 245–281
2 Haeberle, S., Zengerle, R.: 'Microfluidic platforms for lab-on-a-chip applications', *Lab Chip*, 2007, **9**, pp. 1094–1110
3 Song, J.H., Evans, R., Lin, Y.Y., Hsu, B.N., Fair, R.B.: 'A scaling model for electrowetting-on-dielectric microfluidic actuators', *Microfluid Nanofluid*, 2008, **7**, (1), pp. 75–89
4 Lippmann, M.G.: 'Relations entre les phénomènes électriques et capillaires', *Ann. de Chim. et de Phys.*, 1875, **5**, (11), pp. 494–549
5 Young, T.: 'An essay on the cohesion of fluids', *Philos. Trans. R. Soc. Lond.*, 1805, **95**, pp. 65–87
6 Lee, J., Moon, H., Fowler, J., Schoellhammer, T., Kim, C.J.: 'Electrowetting and electrowetting-on-dielectric for microscale liquid handling', *Sens. Actuators A*, 2002, **95**, pp. 259–268
7 Pollack, M.G., Shenderov, A.D., Fair, R.B.: 'Electrowetting-based actuation of droplets for integrated microfluidics', *Lab Chip*, 2002, **2**, pp. 96–101
8 Young, P.M., Mohseni, K.: 'Calculation of DEP and EWOD forces for application in digital microfuidics', *J. Fluids Eng.*, 2008, **130**, (8), pp. 081603 (9 pages)
9 Zeng, J., Korsmeyer, T.: 'Principles of droplet electrohydrodynamics for lab-on-a-chip', *Lab Chip*, 2004, **4**, pp. 265–277
10 Berthier, J., Dubois, P., Clementz, P., Claustre, P., Peponnet, P., Fouillet, Y.: 'Actuation potentials and capillary forces in electrowetting based microsystems', *Sens. Actuators A*, 2007, **134**, pp. 471–479
11 Berthier, J.: 'Microdrops and digital microfluidics', (William Andrew Publishing, Norwich, NY), p. 199
12 Jang, L.S., Hsu, C.Y., Chen, C.H.: 'Effect of electrode geometry on performance of EWOD device driven by battery-based system', *Biomed. Microdevices*, 2009, **11**, (5), pp. 1029–1036
13 Wang, G., Teng, D., Fan, S.-K.: 'Digital microfluidic operations on micro-electrode array architecture'. IEEE Int. Conf. on Nano/Micro Engineered and Molecular Systems, Kaohsiung, Taiwan, February 2011, pp. 1227–1230
14 Fowler, J., Moon, H., Kim, C.J.: 'Enhancement of mixing by droplet-based microfluidics'. Proc. Conf. IEEE Micro Electro Mechanical Systems (MEMS), Las Vegas, USA, January 2002, pp. 97–100
15 Ottino, J.M.: 'The kinematics of mixing: stretching, chaos, and transport' (Cambridge University Press, Cambridge, 1989), pp. 119–122

© The Institution of Engineering and Technology 2011

doi: 10.1049/iet-nbt.2011.0018